Interdependence of Radiation and Microphysics in Cirrus Clouds

V. RAMASWAMY* AND A. DETWILER

*Advanced Study Program, National Center for Atmospheric Research,** Boulder, CO 80307*

(Manuscript received 30 August 1985, in final form 25 March 1986)

ABSTRACT

The important microphysical relationships determining the radiative properties and growth of ice crystals in stratiform cirrus clouds are investigated. A horizontally infinite cloud layer is modeled in the midlatitude upper troposphere. Optical properties of spheres of equal surface area are assumed to represent the scattering characteristics of nonspherical crystals, while the delta-Eddington approximation is used to solve the radiative transfer equations.

Classical expressions for ice particle growth and sublimation are coupled to those for radiative energy exchange in order to follow ice particle evolution within the cloud. The radiative properties of the clouds influence the balance among the cloud physical processes within the cloud. In the top 5 percent of optically thin clouds, the ice particle energy balance is essentially between latent and heat diffusion. In the case of clouds with large optical depths, the energy balance is between latent heat and radiation, i.e., radiative cooling enhances particle growth by vapor deposition. In the lower 5 percent of optically thin or thick clouds, latent heat and radiation are balanced by the diffusion of heat from the particle to the environment. Here, upwelling radiation enhances particle sublimation at cloud base. Environmental ice saturation ratio is the primary factor determining the energy balance during growth of ice crystals. When the ice saturation ratio is ~ 1, crystal growth rates are small, and radiative heating/cooling exercises a strong influence. However, for ice saturation ratios more than a percentage above or below unity, radiative influences on growth rates of crystals with lengths less than 200 μm are negligible.

We have followed the one-dimensional temporal evolution of 1-km thick cirrus cloud layers subsiding in still air. Crystals at cloud top grow larger with time while those at cloud base sublimate as the cloud settles into dry air, with the vertical fall distance greater for larger initial crystal lengths. The temporal evolution of the cloud microphysical characteristics results in modification of the radiation fields, both within the cloud and at the cloud boundaries.

1. Introduction

Clouds composed of ice crystals (cirrus clouds) occur frequently in saturated regions of the upper troposphere. They form as a result of in situ vertical motions in this region and also as "exhaust plumes" from deep convective clouds that extend vertically from the lower to the upper troposphere. Although often tenuous, these clouds can be extensive and long-lived. Cirrus clouds play an integral role in various atmospheric processes. Cirrus radiative properties are important modulators of incoming solar and outgoing planetary radiation (Manabe and Wetherald, 1967; Liou, 1973; Stephens, 1980; Ramanathan et al., 1983). Crystals falling from them may seed lower supercooled liquid water clouds and influence precipitation formation (Braham and Spyers-Duran, 1967). They may also influence tropopause formation and precipitate water from the stratosphere (Goody, 1964; Danielsen, 1982).

Over the past decade, there have been several theoretical studies of cirrus clouds. Heymsfield (1975a,b) has observed and modeled cirrus uncinus generating cells with prescribed wind fields. Hall and Pruppacher (1976) and Stephens (1983) have studied the influence of radiation on the growth and evaporation of single crystals. Wendling (1980) investigated the effects of longwave radiation on particle growth in static cirrus layers. Welch et al. (1980a) examined the radiative properties of ice crystals and cirrus layers at the solar wavelengths. Starr and Cox (1985) have studied convective cirrus cloud cells using a bulk parameterization of longwave and solar radiative properties based on ice water content.

Measurements within cirrus clouds show a wide range of particle shapes, sizes and concentrations. Sizes range from submicron to several millimeters, while concentrations may exceed 1000 L^{-1}. Some of these measurements are summarized in Heymsfield and Platt (1984). Cloud microphysical properties can vary widely between clouds that superficially appear to be of the same type, and even over distances of a few hundred meters within the same cloud. Owing to the complexity of the various physical processes involved in the generation, maintenance and decay of cirrus clouds, the modeling efforts have to proceed from simple approx-

* Present affiliation: Geophysical Fluid Dynamics Program, Princeton University, Princeton, NJ 08540.

** The National Center for Atmospheric Research is sponsored by the National Science Foundation.

imations. These efforts have to be hierarchical in nature, with each successive one offering new perspectives into the physical processes associated with cirrus clouds.

We discuss here a study of the interactions between the microphysical and radiative energy exchanges in cirrus clouds. We consider cirrus layers containing monodispersed randomly oriented bullet-shaped ice crystals in the size range 75 to 300 μm. These sizes are typical of the cross-sectional mean sizes in many cirrus clouds. Although ice crystals in cirrus clouds have a wide variety of shapes and are polydispersed, we simplify the analysis here by restricting our considerations to a single shape and monodispersed size distributions. We assume, for the purposes of the present sensitivity study and from the viewpoint of convenience and simplicity, that the optical properties of the bullets can be represented by spheres of equal surface area (section 2). The radiative properties of the ice clouds are evaluated using the delta-Eddington approximation to the radiative transfer equation (section 3). It is shown there how cloud crystal lengths and concentrations are important in determining the solar and the longwave fluxes inside the cloud and at the cloud boundaries. Variations in sizes and concentrations, thus, affect the cloud-top cooling rate, cloud-base heating rate and the solar reflectivity and absorptivity.

The roles of radiative and thermodynamic forcing during the growth or sublimation of crystals are investigated using mass and energy balance equations (section 4). The effects of varying supersaturation and optical depth on the radiative, latent and diffusive fluxes to particles inside cirrus clouds are assessed. Microphysical processes are considered explicitly throughout the cloud. We consider ice crystal concentrations in evolving cloud layers and evaluate the energy balance at cloud top and base. This is in contrast to the earlier studies (Wendling, 1980; Stephens, 1983), where static cloud layers or the evolution of a single crystal were considered. The influence of crystal growth on the depletion of vapor in the cloud environment is discussed in section 5. The temporal evolution of the cloud microphysical and radiative quantities are analyzed in section 5 for simple idealized cirrus cloud layers.

2. Ice crystal optical parameters

Ice crystals occurring in the atmosphere exhibit a great variety of platelike, columnar and dendritic shapes with predominantly hexagonal symmetry. Columns with pyramid-shaped tips (bullets) are predominant at temperatures below −25°C (Heymsfield and Platt, 1984). The problem of scattering by crystals of such diverse shapes in different orientations is formidable. Thus far, only geometrically equivalent spheres or right circular cylinders have been employed for ice crystal scattering calculations (Liou, 1974; Hunt, 1973; Stephens, 1980). For purposes of simplicity, we choose to consider bullet-shaped crystals in random orientation and consider their scattering characteristics in terms of surface area equivalent spheres. This approximation is adequate for flux calculations of the accuracy required for the present study. We can write the optical cross sections for a given wavelength as

$$\sigma_i = \pi r_{ES}^2 Q_{ES,i} \tag{1}$$

where i = 1, 2 or 3 (for extinction, scattering and absorption, respectively), Q denotes the corresponding optical efficiency, r is the radius (Q is calculated from the Mie theory for a sphere of equal surface area, using the refractive indices given by Warren, 1984) and ES denotes sphere of same surface area as the ice bullet. The dimensions of the equivalent sphere (r_{ES}) are calculated from the surface area (S_N) of bullet-shaped ice crystals (i.e., hexagonal columns with tipped ends):

$$r_{ES} = \frac{(S_N)^{1/2}}{4\pi}. \tag{2}$$

Based on an empirical relationship (Heymsfield, 1972), we formulate

$$S_N = 0.0334L^{1.572} + 0.505L^{1.786} \tag{3}$$

where L (cm) is the length of the crystal. Also, the mass of the crystal M (gm) is given by

$$M = 0.0137L^{2.572}. \tag{4}$$

For a homogeneous cloud of geometrical thickness Z and comprising monodispered ice crystals with length L and concentration n, the vertical ice water path is given by

$$\text{IWP} = M(L)n(L)Z. \tag{5a}$$

The optical depth (δ) is determined both by lengths (L) of the crystals and their concentration (n). Thus, for a homogeneous cloud, the optical depth is given by

$$\delta(L) = \sigma_1(L)n(L)Z. \tag{5b}$$

The specific optical parameters (ψ) are defined as (Ramaswamy and Kiehl, 1985) the ratio of the respective optical cross section to the mass. Thus, for example, the specific extinction is defined as

$$\psi_1 = \frac{\sigma_1}{M} = \frac{\delta}{\text{IWP}}. \tag{5c}$$

For randomly oriented crystals of given density, the specific extinction, for example, decreases with increasing length at all wavelengths. We also note here that the single scattering albedo (ω) is defined as the ratio of the energy not absorbed by the crystals to the incident energy at each scattering event.

3. Transfer of radiation

We employ the delta-Eddington approximation (Joseph et al., 1976) to calculate the radiative fluxes at both solar and long wavelengths. The application of

this method for solar radiation has been developed in detail by Joseph et al. (1976) and Coakley et al. (1983). In appendix A, we describe the application for the longwave spectrum.

The transfer in the solar spectrum involves 56 spectral intervals, with 47 of these in the visible and nine in the near-infrared. In the present study, the cloud is located between 10 and 11 km in a McClatchey (1972) midlatitude summer atmosphere. The up- and downward solar fluxes are calculated using the model described in Ramaswamy and Kiehl (1985), with the obvious difference being the introduction of a cirrus cloud instead of the water cloud. The cloud single-scattering properties in each wavelength interval are determined according to the equivalent sphere approximation mentioned in section 2. Near-infrared water vapor absorption is evaluated using the exponential fits of Liou and Sasamori (1975). Saturation within the cloud with respect to water is assumed to be unity for purposes of water vapor absorption calculations. The integrated solar irradiance input at the top of the atmosphere is 1360 W m^{-2} while the cosine of solar zenith angle is assumed to be 0.5. Surface albedo is assumed to be 0.1.

In the longwave spectrum, we perform the calculations in the window (8–12 μm) region only, following Stephens (1983). Because of the geometrical optics assumption invoked in section 2, the calculation of the single scattering properties at a single wavelength can be expected to yield representative values for the ice crystals' behavior in the entire longwave spectrum. Such a calculation, in contrast, is not possible in the solar spectrum because of variations in the scattering optical depth across the spectrum. Scattering is explicitly accounted for in the longwave, as shown in appendix A. The longwave fluxes inside the cloud and at the cloud boundaries require a knowledge of the flux incident at the top ($\delta = 0$) and at the base of the cloud ($\delta = \delta_f$). These boundary conditions are prescribed as

$$F^{\downarrow}(\delta = 0) = 30\ \mathrm{W\ m^{-2}} \tag{6}$$

$$F^{\uparrow}(\delta = \delta_f) = 275\ \mathrm{W\ m^{-2}}. \tag{7}$$

These values were obtained as clear sky fluxes from the model of Ramaswamy and Kiehl (1985). The cloud top temperature is fixed at 224.5 K and the cloud base temperature at 231.5 K. In the layers containing ice crystals, only the particulate radiative effects are considered, i.e., the longwave properties of gases are ignored. The assumption is made possible by the smaller opacity of water vapor and CO_2 relative to that of ice crystals within the atmospheric window and at the altitude in question (see Paltridge and Platt, 1976). In the present analysis, we consider only the effects inside and at the cloud boundaries. We do not consider the feedback effects on the rest of the atmosphere and the subsequent modification of the fluxes incident at the cloud boundaries. Also we do not consider clouds at other altitudes. We have instead chosen to concentrate on how clouds with different microphysical characteristics evolve in a specific environment.

The cloud is subdivided into 20 layers, each 50 m thick. This fine resolution is necessary for the investigations of the microphysical processes discussed later. Crystals in all layers are assumed to have the same lengths initially.

a. Sensitivity of radiation fields to cloud properties

The parameters specifying the cloud properties are crystal length and concentration, and the ice water path of which two are independent variables. The sensitivity of the radiative properties can be examined by treating any of these three characteristics as the dependent variable. The sensitivity of the radiation fields to variations in cloud physical properties is examined here from the perspective of constant ice water path. For a constant ice water path, a cloud containing smaller crystals has a higher specific extinction than one containing larger crystals; the former also has a higher particle concentration and a higher optical depth (see Eq. 5).

The cloud top radiative cooling (Q_F) in the uppermost 50 m (i.e., top 5 percent) of the cloud is shown in Fig. 1 for monodispersed clouds as a function of ice water path. We select lengths of 75, 100 and 200 μm which correspond to typical cross-sectional mean lengths for ice crystal distributions observed in the atmosphere (Heymsfield and Platt, 1984). The range of ice water paths and lengths chosen ensure that the concentration lies between 0.01 and 1.0 cm^{-3}. For an ice content of 20 gm m^{-2}, a cloud containing crystals of length 75 μm yields four times higher cooling at cloud top than a cloud containing crystals of length 200 μm.

b. Solar radiation

The influence of crystal sizes on solar radiation is shown in Fig. 2. Clouds comprised of crystals having

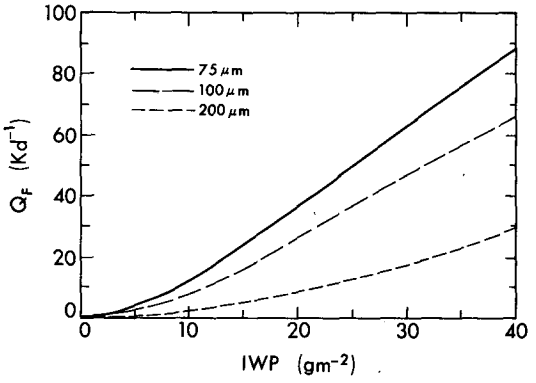

FIG. 1. Longwave cooling rate (Q_F) in the upper 50 m of a 1-km thick cirrus as a function of column ice content for clouds containing crystals of lengths 75, 100 and 200 μm, respectively.

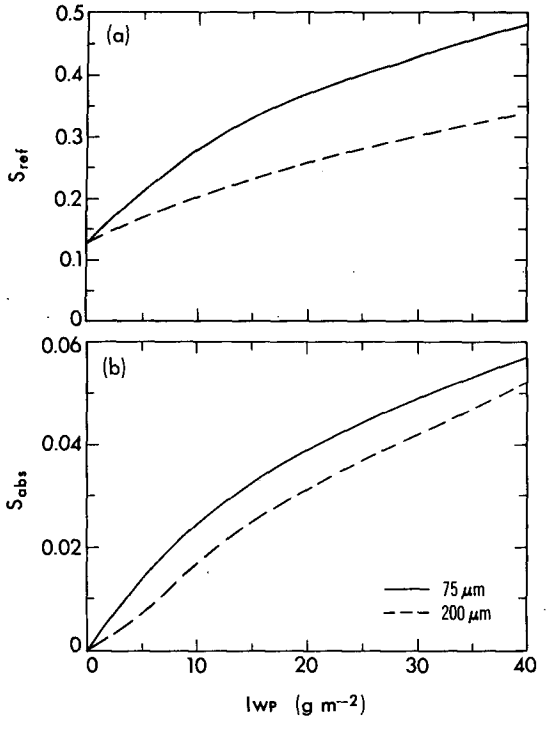

FIG. 2. Solar (a) reflectivity (S_{ref}) and (b) absorptivity (S_{abs}) as a function of the cloud ice content in 1-km thick clouds containing crystals of lengths 75 and 200 μm. Cosine of solar zenith angle is 0.5.

a length of 75 μm have a higher solar absorptivity (S_{abs}) (Fig. 2a) and a higher solar reflectivity (S_{ref}) (Fig. 2b) for the same ice water path than crystals of length 200 μm. For any ice water path, changes in crystal length are more significant in causing changes in the reflection of radiation than in its absorption because of the approximately dielectric properties of ice in the solar spectrum. For example, for constant ice water path of 20 gm m^{-2}, as the crystal length increases from 75 to 200 μm, the reflectivity changes from 0.36 to 0.26 while the absorptivity changes from 0.039 to 0.031. Similar trends are also revealed in the calculations of Welch et al. (1980b).

c. *Cloud top and cloud base*

The solar and longwave heating rates at cloud top for a constant ice water path of 20 gm m^{-2} are shown in Fig. 3a as a function of crystal length. For the altitude considered (10–11 km), the longwave cooling dominates over the solar heating for lengths less than 250 μm and this is more pronounced for the smaller sizes, where the specific extinction and thus the optical depth are large. The solar heating for a crystal length of 75 μm is 10 K day^{-1} compared to the longwave cooling of 35 K day^{-1}. With an increase in the crystal length for a constant cloud ice content, the number of crystals decreases, lowering the cloud optical depth [Eq. (5b)]. This results in layers near the cloud top "sensing" more of the radiation incident from below the cloud base; the longwave cooling is thus reduced for the larger crystals. The optical depth in the solar spectrum also decreases with length; however, this results in a smaller decrease in the solar heating relative to the decrease in the longwave cooling. The difference between the magnitudes of the solar and the longwave convergences is a direct consequence of the higher absorptivity in the longwave. Note that, in contrast to the solar absorption, the solar reflection exhibits a larger sensitivity due to changes in crystal length, as seen in Fig. 2.

For very thin clouds, solar heating can compensate completely for and even exceed the longwave cooling at the cloud top. The optical depth at which this cancellation occurs depends on the altitude of the cloud and, thus, on the latitudes and season. Tropical cirrus, which are found at higher altitudes (colder temperatures), would exhibit a larger cooling than a midaltitude cloud of comparable characteristics. Hence, the optical depth where the compensation effect occurs would shift to lower values in the case of the tropical cirrus.

Similar arguments hold for the radiative heating rates at the cloud base (Fig. 3b). Again, with decreasing crystal length and for a constant ice content, the decreases in the longwave heating rates are greater relative to

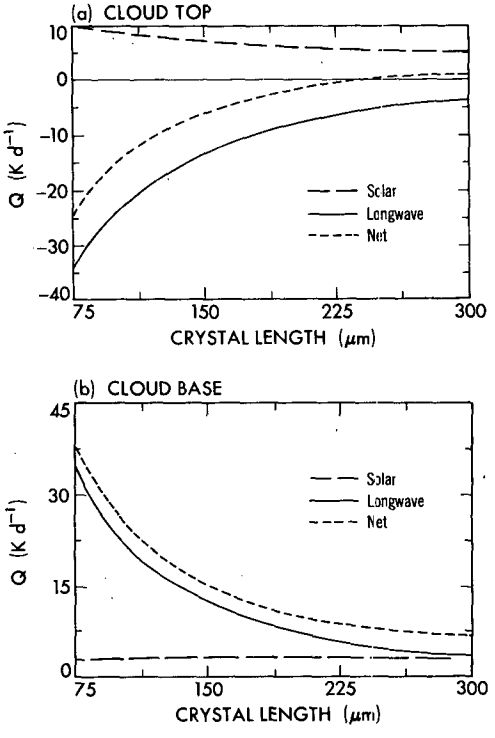

FIG. 3. Solar, longwave and net heating rates at (a) cloud top and (b) cloud base in 1-km thick clouds containing crystals of different lengths. Cloud ice water path is fixed at 20 gm m^{-2} and layers 50 m thick are considered. Cosine of solar zenith angle is 0.5.

decreases in the solar heating rates. With decreasing optical depth, the crystals at the cloud base are more efficient in radiating to space. The magnitude of the warming of the cloud base would depend on the surface temperature (e.g., the diurnal cycle of continental surface temperature), water vapor amounts in the lower and midtroposphere and the continuum absorption.

The net effect at cloud base is one of heating while at the top it is one of cooling (for large optical depths) for the conditions assumed. For large optical depths, the solar radiative processes are overshadowed by the longwave processes both at the base and at the top of the cloud. The results shown in Figs. 1–3 also illustrate the uncertainty introduced when cloud radiative properties are parameterized as a single-valued function of the ice water path.

4. Thermodynamic-radiation interaction

The details of ice crystal growth (or sublimation) in the cloud environment discussed in section 3 are examined next. The equations governing crystal growth follow those described by Barkstrom (1978). Particle growth is constrained by the conservation of water mass and total energy at the particle surface. For crystals of a specific length L, the balance is prescribed by

$$\frac{dM}{dt} + 4\pi C D f_1 \Delta\rho = 0 \tag{8}$$

$$L_p + R_p - C_p = 0 \tag{9}$$

with

$$L_p = L_s \frac{dM}{dt} \tag{10}$$

$$R_p = S_p + F_p = \frac{(S_{\text{div}} + F_{\text{div}})}{n} \tag{11}$$

$$C_p = 4\pi C K f_2 \Delta T \tag{12}$$

where M is mass, t is time, C is the capacitance (equivalent radius for diffusive processes) of a bullet-shaped crystal, D is the diffusion coefficient for water vapor, K is the diffusion coefficient for heat and f are factors describing the enhancement of vapor and heat transport due to ventilation during fall and due to high surface curvature if the particles are very small, $\Delta\rho$ is the difference in vapor density between the equilibrium value at the surface temperature and the environmental value and L_s is the latent heat of sublimation (assumed constant), R_p is the rate of radiant energy gained per crystal, while S_{div} and F_{div} represent the convergences due to solar and longwave radiation, due to crystal absorption, n the number concentration of particles, C_p the diffusive heat flux to the crystal and ΔT the temperature difference between the particle and the environment. The subscript "p" denotes specific quantities for individual crystals.

The analytical expressions for the mass growth rate and particle temperature, at equilibrium, are derived by solving (8) and (9) simultaneously. The solutions are identical to those derived by Barkstrom for growth of water drops but neglecting solute effects. Using a linearized form of the Clausius–Clapeyron equation for equilibrium water vapor pressure as a function of temperature, the ideal gas law and Kelvin's expression for vapor pressure are combined to yield, after some algebra, the following equations for particle growth and particle-air temperature difference:

$$\frac{dM}{dt} = \frac{A_2 C S' - A_4 R_p}{A_5} \tag{13}$$

$$\Delta T = T_{\text{particle}} - T_{\text{ambient}} \tag{14}$$

$$= \frac{L_s S' + (R_p / C A_1)}{A_5} \tag{15}$$

where

$$S' = (S - 1) - A_3 \tag{16}$$

$$A_1 = 4\pi f_1 D \frac{e_s}{R_w T} \tag{17}$$

$$A_2 = 4\pi f_2 K \tag{18}$$

$$A_3 = \frac{2s}{\rho_i R_w T r} \tag{19}$$

$$A_4 = \frac{L}{R_w T^2} \tag{20}$$

$$A_5 = \frac{L_s^2}{R_w T^2} + \frac{f_2 K R_w T}{f_1 D e_s} \tag{21}$$

and S is the ice saturation ratio, s the surface free energy of ice, ρ_i the bulk ice density, T temperature (K), R_w the gas constant for water, r is half of the particle width and e_s is the saturation vapor pressure at temperature T; S' describes the effective thermodynamic driving force for growth, while $A_4 R_p$ and $R_p / C A_1$ describe the effect of radiative heating on particle growth rate and temperature. The expressions for the diffusivity of vapor and heat and the combined ventilation and curvature factors f_1 and f_2 are taken from Pruppacher and Klett (1978). Equation (13) is basically the classical particle growth rate equation (Howell, 1949) with the addition of a radiative energy term.

To examine the role of radiative, latent heat and diffusive processes, we define

$$\alpha_R = \frac{A_2 C S'}{A_4 R_p} \tag{22}$$

$$\beta_R = \frac{L_s S'}{R_p / C A_1}. \tag{23}$$

Essentially, α_R compares the thermodynamic and radiative forcing in the growth rate of crystals while β_R

compares the thermodynamic and radiative processes in setting up the temperature difference between the crystal and environment.

For example, we consider the behavior of α_R in different supersaturation regimes for the case of the 1 km cloud discussed in section 3. The crystal length is 200 μm, the concentration 0.033 cm^{-3} such that the ice water path is 20 gm m^{-2}. We find then from Fig. 4a that α_R is less than 1, i.e., the net radiative forcing (combined solar and longwave effects) dominates the thermodynamic forcing in the mass growth relation (13), for saturation ratios between 0.97 and 1.03. Within this restricted range of ice saturation ratio, growth may occur in subsaturated conditions due to radiative cooling (cloud top) or sublimation may occur in supersaturated conditions due to radiative heating (cloud base). For values of S outside this regime, saturation ratio dominates the growth or sublimation process. For example, in the foregoing case, if the value of S is 0.8 or 1.2, the thermodynamic forcing exceeds the radiative forcing by a factor of 26. This behavior is to be compared to that for large crystals ($\sim$800 μm; see Stephens, 1983), where because of the large surface area, radiation is significant for any saturation ratio.

The effects of radiation on the crystal air temperature difference (β_R) are significant for a wider range of ice saturation ratios than for α_R (Fig. 4b). The radiative energy is significant in determining the temperature difference between the particle and the environment for $0.89 < S < 1.1$, i.e., radiation contributes more than the thermodynamic process to ΔT. Even at a value of S equal to 0.8 or 1.2, the thermodynamic forcing exceeds the radiative forcing by only 20 percent. Therefore, for any specific saturation ratio, when compared with the magnitude of the thermodynamic term, radiation has a relatively more significant influence on the diffusive energy exchange between crystal and environment than on the crystal growth rate.

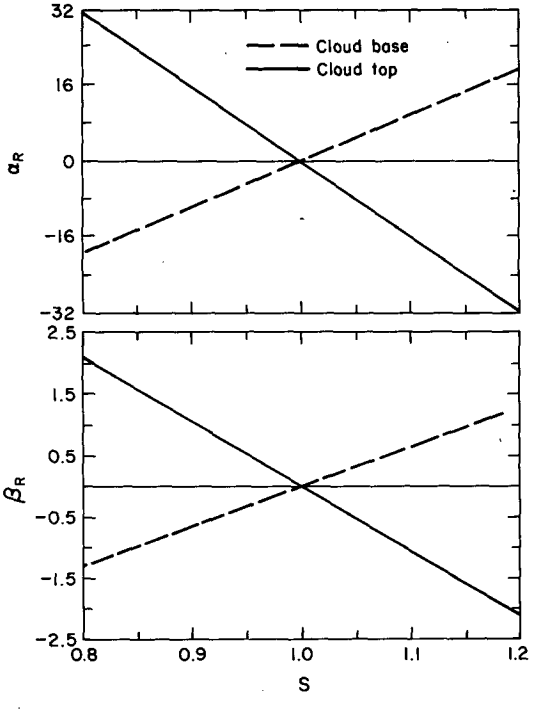

FIG. 4. Ratio of the thermodynamic to radiative forcing during daytime in (a) the growth rate of crystals (α_R) and (b) the crystal-air temperature difference (β_R). Crystal length is assumed to be 200 μm while the concentration is 0.033 cm^{-3}.

It is evident that crystals developing in different saturation regimes in the atmosphere will have different growth rates and different balances between the radiation and thermodynamic processes. Supersaturation will occur in strong updrafts, particularly with low crystal concentrations. Ice saturation ratios will be approximately 1 in regions of weak vertical motion and high crystal concentrations. Such regimes, which see only slow crystal growth or sublimation, experience a proportionately large radiative influence due to cooling (at cloud top) and heating (at cloud base).

a. Microphysical energy exchanges in cloud

The microphysical exchanges involving the thermodynamic and the radiative processes in a 1 km thick cloud are investigated by assuming the cloud to consist of a vertical stack of 20 layers, each with a homogeneous population of bullet-shaped ice crystals. Air temperature, water vapor density, crystal length and concentration are assumed to be constant in any layer. We investigate first the magnitudes of the radiative, latent heat and diffusion terms in the nonisothermal cloud with the following initial conditions. The ice saturation ratio in the cloud is 1.2. Particle concentration (0.033 cm^{-3}) and length (200 μm) are the same for each layer. The radiative calculations follow the description in section 3.

The vertical profiles of radiative, latent and diffusive fluxes, are delineated in Fig. 5 in terms of the power delivered to or from a crystal at different vertical locations in the cloud (measured downwards from the cloud top). The radiative energy per crystal is denoted by F_p (longwave) and S_p (solar), the diffusive energy by C_p and the latent heat energy by L_p. First, it is important to consider the situation in the absence of radiative fluxes. In this case, the latent heat release due to crystal growth will be balanced by diffusion of heat away from the crystal and there would be no vertical gradients in either the latent heat or the diffusive heat fluxes inside the cloud. For example, when S is 1.2, then the magnitudes of the two fluxes will be 1.35 microwatts per crystal everywhere within the cloud for the case examined in Fig. 5.

In Fig. 5a, the profiles are shown of the fluxes within a cloud in the presence of longwave radiation only (nighttime case). At cloud top, relative to the no-ra-

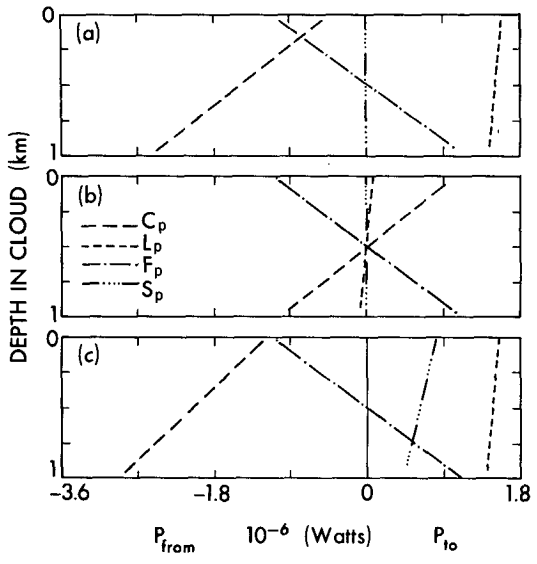

FIG. 5. Disposition of solar (S_p), longwave (F_p), latent (L_p) and diffusive (C_p) power flowing from (P_{from}) or to (P_{to}) crystals in different layers of a 1-km thick cirrus cloud. Crystal length is 200 μm and the ice content is 20 gm m^{-2}. Depth of cloud is measured downwards from cloud top. (a) Nighttime conditions with ice saturation ratio 1.2; (b) nighttime conditions with ice saturation ratio 1.0; and (c) daytime conditions with ice saturation ratio 1.2.

diation case, there is an increase in the latent heat release caused by an increase in the growth rate (due to radiative cooling). However, as shown above, radiative effects on the growth rate for $S = 1.2$ are small. Similarly, at cloud base, radiative warming effects are overwhelmed by the effects of supersaturation on crystal growth. Thus, the latent heat release throughout the cloud is almost the same as that in the absence of radiation. The major effect due to the longwave radiation is on C_p. The cooling at the top results in lower crystal temperature (approximately 0.04 K cooling) and a reduced diffusion of heat to the environment compared to the case when radiative effects are not considered. At cloud base, similarly, the diffusion of heat to the environment is greater than in the absence of radiation (crystal warming approximately 0.07 K). As to be expected from prior discussions, the differences in the diffusive heat fluxes at cloud top and cloud base are quite large (e.g., an increase in the diffusive power of 1.8 microwatts per crystal at cloud base). The longwave cooling and diffusion of heat away from the crystals balance latent heating at the top, while longwave heating and latent heat balance diffusion of heat away from the crystal at cloud base.

We next illustrate the case when $S = 1.0$ (Fig. 5b) and during nighttime. Compared to Fig. 5a, the latent heat release is dramatically reduced (i.e., growth rates are small) despite radiative cooling at the cloud top. Similarly, at cloud base, the latent heat term is small and radiative warming causes the sublimation of crystals (i.e., latent heat transfer is directed from ambient air to crystal). Radiative energy emission/absorption is nearly balanced by diffusion heating/cooling. Note that even though cloud boundary crystal growth/sublimation rates are small, they are large percentagewise compared to the zero growth rate expected for $S = 1$. This is discussed after Eq. (22) where the relative importance of supersaturation and radiation in determining particle growth is described.

The case when both solar and longwave radiative exchange take place (daytime) is considered for $S = 1.2$ in Fig. 5c. Since the solar flux absorbed is small in magnitude compared to the longwave, only small changes take place in the latent and diffusive fluxes, compared to the results shown in Fig. 5a.

The effect of the extra power delivered to the crystal through absorption of solar radiation (which decreases from the top of cloud towards base) is compensated by the increase of the diffusive flux from the particle to the environment.

In general, the latent heat release decreases by a small amount from cloud top to cloud base due to decrease in the growth rate. This is primarily a consequence of longwave flux convergence, which is greater near cloud base than near cloud top. However, if the supersaturation in the cloud is high, the latent heat term is positive throughout, even at cloud base; C_p [proportional to $(T_{\text{particle}} - T_{\text{ambient}})$; see (12) and (14)] is positive throughout the cloud and heat is conducted away from the crystals everywhere within the cloud, with the amount conducted away increasing towards cloud base.

b. *Effect of crystal concentrations*

No unique relationship exists between crystal sizes and concentrations in cirrus clouds. We examine here the effects of different optical depths, as determined by crystal concentrations. The resulting changes in the energy balance in the various cloud levels alter energy convergences (or divergences). The influences of the radiative, diffusive and latent heat processes on the heating/cooling rates (in 50 m deep layers) at cloud top and cloud base as a function of crystal concentration (n) [or, equivalently, the optical depth via (5)] are shown in Fig. 6. The length of the crystals is fixed at 200 μm; Q_R, Q_L, Q_C denote the net radiative (sum of solar and longwave), latent and diffusive heating rates.

For the case when $S = 1.2$ (Fig. 6a), at cloud top, Q_R is negative (cooling) and decreases steadily with increasing optical depth due primarily to increase in the longwave flux divergence. Because growth rates are large ($S = 1.2$), the latent heat released increases with increasing concentration so that, excepting at small concentrations, the latent heat and radiative cooling compensate each other. At cloud base (Fig. 6b) crystals grow in the supersaturated environment, making Q_L positive despite radiative heating. In fact, Q_L increases with increasing concentration, as does Q_R. To balance

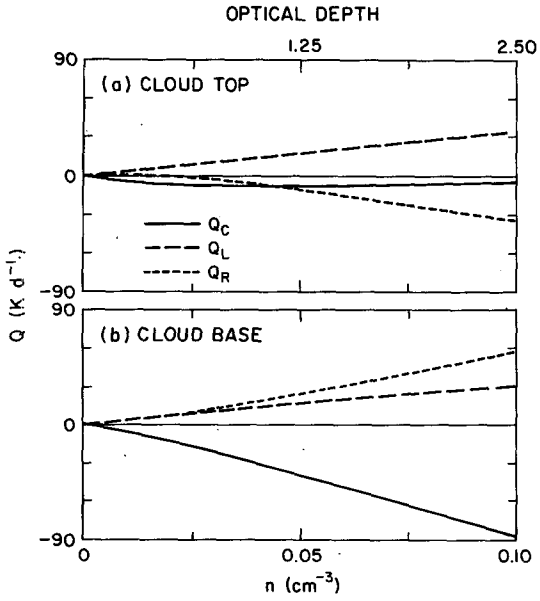

FIG. 6. Heating rates (daytime) due to net radiative (Q_R), diffusive (Q_C) and latent heat flux (Q_L) convergences in a 1-km thick cloud as a function of crystal concentration (or, equivalently, optical depth). Crystal length is assumed to be 200 μm and ice saturation ratio 1.2. (a) For a 50-m thick layer at cloud top; (b) for a 50-m thick layer at cloud base.

radiative heating and latent heat release, Q_C becomes large and negative with increasing concentrations and this heat is conducted away from the crystal.

5. Temporal evolution of physical parameters

In sections 3 and 4, the microphysical factors affecting the radiative processes and the growth (or sublimation) of ice crystals at low temperatures ($T \sim 228$ K) were examined individually. In this section, the interactions among the various factors are investigated by considering the evolution of a one-dimensional model cirrus cloud over 40 minutes. We consider a simple stratiform cloud that is 1 km thick initially, is of infinite horizontal extent and bereft of turbulent motions. The objective here is to distinguish the important physical changes that accompany cloud evolution during the initial periods. The methodology involved in performing the simulation is described in appendix B. The initial conditions chosen are a particle concentration of 0.033 cm^{-3} of 200 μm bullets. The ice saturation ratio in the layer is initially 1.2 and below cloud it is 0.9. Air temperature (228 K) and pressure (250 mb) are everywhere the same initially. Pressure is held constant during the simulation although temperature may change with time. Pressure influences primarily the diffusivity terms in the crystal growth equation and aerodynamic drag in the fallspeed equation. Holding the pressure constant is not a severe restriction for a 1 km cloud over the time scales considered below.

In the simulation, some convective motion can be pictured as having set up an initially humid layer in which ice nucleation occurs as liquid water saturation is approached. This is a realistic assumption at low temperatures in the upper troposphere (Heymsfield, 1973; 1975a). Crystals are assumed to appear simultaneously everywhere within the cloud. Rapid particle growth follows nucleation since there is a relatively large supersaturation with respect to ice and particles quickly grow large enough to settle against the weak upward motions which set up the supersaturation. Thus, the simulation aims to capture the essence of horizontally extensive cirrus cloud evolution in layers with weak or no upward motion.

The temporal evolution of the positions of the upper and lower cloud boundaries and maximum and minimum crystal size are shown in Figs. 7 and 8, respectively. Ice particles grow in the initially supersaturated layer and fall into dry air below. Once in the dry air the lowest cloud layers begin to sublimate leading to decreases in particle sizes in these lower layers (Fig. 8). The gross behavior observed is that, due to the larger crystals and thereby the higher fallspeeds in layers near the top, the cloud top tends to collapse onto the bottom (Fig. 7). Thus, cloud thickness is halved at the end of 40 min. The cloud has fallen out of the initially supersaturated layer by the end of the period and is sublimating everywhere. Crystal lengths, which are initially 200 μm, are relatively large (223 μm) near cloud top, compared to those at the bottom (117 μm), in the latter stages of cloud evolution (Fig. 8).

The most significant influence on crystal growth is the depletion of vapor in the cloud and the fall of the cloud out of the initial humid layer. The saturation ratio is reduced more quickly (see Table 1) to 1 (in $\sim$5 min) at cloud base than at cloud top. Beyond 20 min, the saturation ratio everywhere within the cloud remains constant. The cloud is at this time slowly sublimating and moistening the drier air below the level of formation. The tendency for the saturation ratio within the cloud to be close to unity implies that the

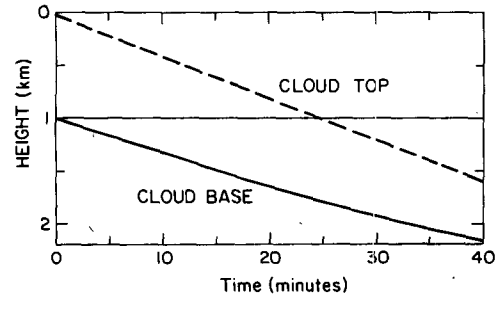

FIG. 7. Evolution of the top and base of a cloud (initial thickness 1-km) containing crystals with an initial length of 200 μm and concentration of 0.033 cm^{-3}. The initial ice saturation ratio within cloud is 1.2 while that below cloud is 0.9.

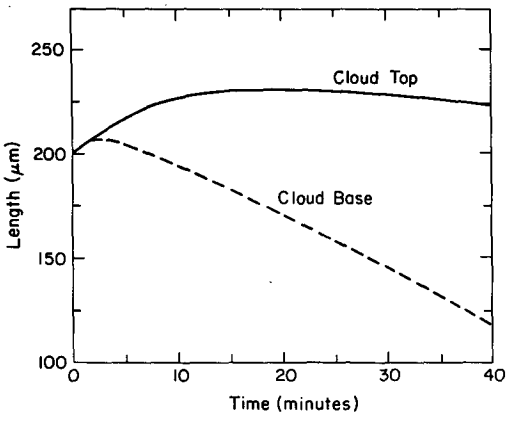

FIG. 8. Maximum (at cloud top) and minimum (at cloud base) crystal lengths in the evolution of the cloud described in Fig. 7.

cloud is brought to a regime where the radiative effects become comparable to or can even dominate the thermodynamic effects in the growth or sublimation of ice crystals [see discussion following Eq. (22)]. The absolute growth or sublimation rates in this regime are, however, small.

a. Changes in cloud parameters

The changes in crystal sizes during the evolution of the cloud imply a change in the optical depth which, in turn, as shown in section 3, will influence the radiative convergences and divergences. This dependence of the cloud physical parameters on crystal sizes and saturation state is highlighted by considering the evolution of four different clouds with different initial specifications. The cloud altitude and temperature are the same in all cases (temperature is 228 K; P is 250 mb). It is assumed, as before, that the initial cloud nucleation has occurred. The four cases considered are as follows:

A: S(cld) = 1.2, S (below) = 0.9, L = 200 μm, n = 0.03 cm^{-3}, identical to the one considered in the previous subsection.

B: Same as A except n = 0.1 cm^{-3}

C: Same as A except S (below) = 0.7

D: Same as A except length = 500 μm, n = 0.01 cm^{-3} and with ice water path similar to B.

Cloud evolution is followed for 40 min and the results are shown in Figs. 9a–c.

The ice water path at different times during the evolution of the cloud is shown in Fig. 9a. Cases A and C, although initialized at identical ice water paths, differ by a factor of 4 at the end of 40 min. The drier air below cloud base in case C causes a higher ice mass to be sublimated. From Table 2, the crystals at the cloud base initially in case C sublimate almost completely after 40 min (length is reduced to 5 μm). Even at cloud top, there exist larger crystals (225 μm) in case A than in case C (100 μm). Due to the presence of the larger crystals for a longer time, the entire cloud in A falls 600 m more than the cloud in C (Table 2).

Cases B and D represent relatively high initial ice water path situations (Fig. 9a). Note that while case B has a higher initial ice content by virtue of high number concentrations, case D has a higher initial ice water path by virtue of a higher mass per crystal. The ice crystals sublimate more slowly in D than in B. The larger crystals in case D lose mass more slowly as they fall into the drier subcloud air because there is less surface area per unit mass of ice than when the same mass is distributed over a large number of smaller crystals. Crystal lengths in D remain fairly large (greater than 440 μm) even after 40 min both at cloud top and cloud base (Table 3). The cloud in case D falls a greater vertical distance (3 km) than any of the other cases owing to a higher fall velocity of the larger crystals. Indeed, this case may be beyond the range of validity of the present model. Because of the higher initial concentration in case B relative to case A, the competition for vapor increases and crystal lengths at cloud top after 40 min are smaller (223 μm in case A versus 210 μm in case B).

b. Changes in radiative parameters

We now consider the changes in albedo and the upwelling longwave flux (F_{CLDTOP}) that accompany the changes in the ice crystals' microphysics. The decrease in ice burden by 5 gm m^{-2} in case A after 40 minutes leads to an increase in the longwave flux (Fig. 9b) at cloud top by about 6 W m^{-2}. Since case C exhibits a reduction in the ice loading from 20 to 5 gm m^{-2} over 40 min, the corresponding change in the longwave flux is higher at cloud top (36 W m^{-2}). Since cases B and D are initialized to nearly equal ice water contents and after 40 minutes still possess substantial loading (case D: 63 to 54 gm m^{-2}; case B: 60 to 45 gm m^{-2}), the longwave flux is almost unchanged between time zero and after 40 minutes. It is pointed out, however, that

TABLE 1. Saturation ratio (S) with respect to ice at different times during the growth of crystals at cloud top and cloud base. Initial supersaturation is assumed to be uniform throughout the cloud. Initial crystal length is assumed to be 200 μm (see Figs. 7, 8 and text).

Time (min)	S (top)	S (base)
0	1.20	1.20
5	1.19	0.92
10	1.05	0.92
15	1.01	0.91
20	0.99	0.91
25	0.97	0.91
30	0.97	0.91
35	0.97	0.91
40	0.97	0.91

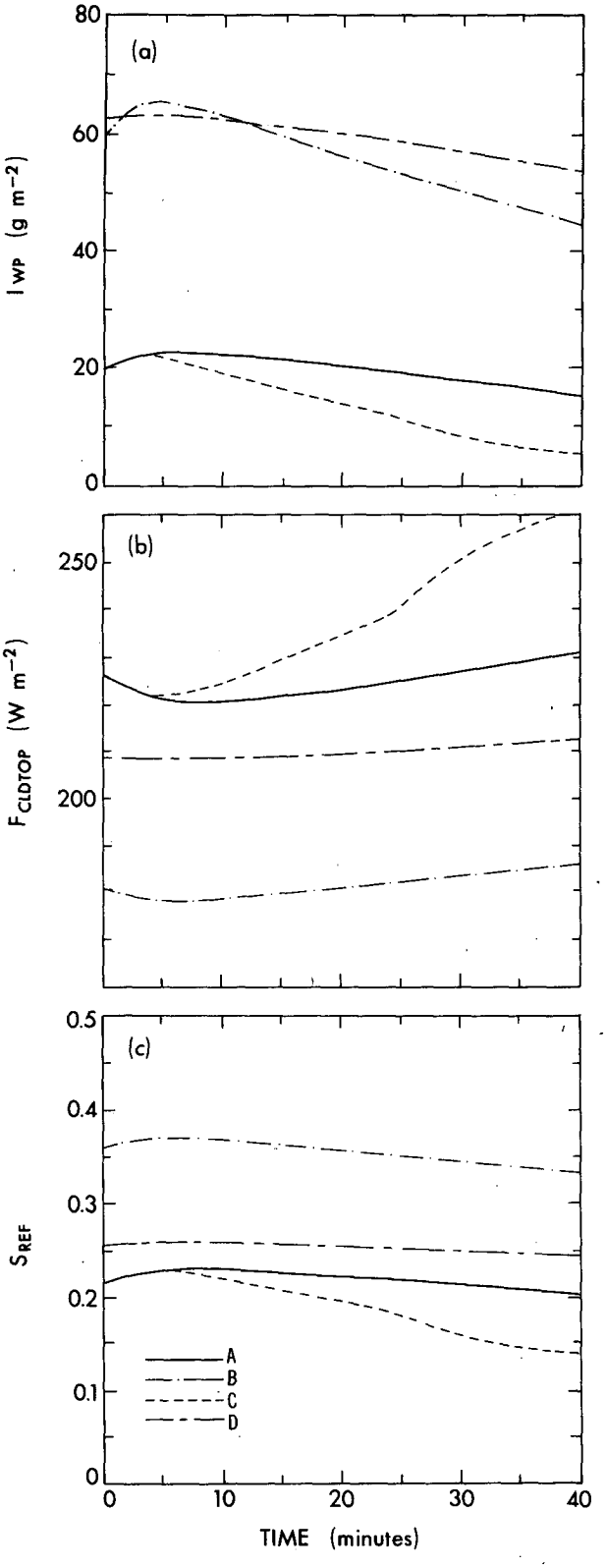

FIG. 9. Evolution of microphysical and radiative parameters in four clouds with different initial specifications. Case A is as shown in Fig. 7. Case C is the same as A except subcloud ice saturation ratio is 0.7 initially. Case B as A except concentration is 0.1 cm^{-3} initially. In Case D, the initial crystal length is 500 μm, the concentration 0.01 cm^{-3} and the ice water path similar to B. Figure shows evolution of (a) ice water path, (b) the emergent longwave flux at cloud top (F_{CLDTOP}), and (c) the solar cloud albedo (S_{ref}).

TABLE 2. Crystal lengths at time zero, after 40 minutes, and the distance fallen by clouds described in Cases A, B, C and D in 40 minutes (see text).

	Length			
Case	$t = 0$ (μm)	at top $t = 40$ (μm)	at base $t = 40$ (μm)	Height fallen (km)
A	200	225	115	1.2
B	200	210	125	1.2
C	200	190	5	1.6
D	500	510	440	3.0

case D differs from B at all times by 28 W m^{-2}. The primary factor for this is the difference in the cloud optical depth. Since mass loadings are similar, the cloud with the smaller crystals will have a larger optical depth and will reduce the upward longwave flux at the cloud top more effectively. The cloud with the smaller crystals will also exhibit a larger radiative divergence at cloud top and a larger radiative convergence at cloud base (see Figs. 1, 3).

The changes in albedo (Fig. 9c) exhibit similar changes as seen for the longwave flux. At the end of 40 minutes, the differences between cases A and C is 0.07 (amounting to a difference in flux of 50 W m^{-2}). Cases B and D differ by ~63 W m^{-2} at all times. The albedo is generally higher for higher mass loadings (Fig. 2) while for a fixed ice content, it is higher for a cloud containing smaller crystals.

The results of this section show that a cloud layer formed in a quiescent environment undergoes significant evolution over short time scales (approximately an hour or less). Although radiative energy may not play an important role in the growth of ice crystals when they form initially in high supersaturation regimes, the evolution of the crystal sizes tends to alter both the short- and longwave radiation fields. In turn, these changes affect the energy balance inside the cloud. The evolution of the cloud microphysical parameters tends to drive the humidity within the cloud to ice saturation, a regime where the radiative effects become more influential relative to the thermodynamic effects.

6. Summary and conclusions

We have investigated the interactions of the latent, diffusive and radiation fields in cirrus clouds for various ice crystal lengths and concentrations and have studied the evolution of the clouds in saturated and unsaturated environments.

TABLE 3. Crystal lengths at time $t = 0$ and after 40 minutes and the distance fallen by clouds described in Cases A, B, C and D (see text) in 40 minutes.

Case	Length ($t = 0$) (μm)	Length (top) ($t = 40$) (μm)	Length (base) ($t = 40$) (μm)	Height fallen (km)
A	200	225	115	1.2
B	200	210	125	1.2
C	200	190	5	1.6
D	500	510	440	3.0

Clouds composed of smaller crystals have higher concentrations and possess a higher optical depth for the same ice content and cloud thickness compared to clouds composed of larger crystals. The variations in the crystal lengths and concentrations are as important as the column ice content in determining the optical depth and the radiative convergences (or divergences).

The interactions between the radiative and the microphysical processes were investigated using mass and energy balance relationships for individual crystals. For the cases examined, growth (or sublimation) rates are primarily determined by ice saturation ratios. Radiative influences on crystal growth (or sublimation) are important only near an ice saturation ratio of unity, where the absolute values of growth (or sublimation) rates are small. Radiative convergences alter the ice crystal energy balance, insofar as the exchange of heat between crystal and environment is concerned. For thin cloud optical depths, heat is diffused away from crystals (i) at cloud top to balance the latent heat release; and (ii) at cloud base to balance the flux convergences due to radiation and latent heat. At large optical depths, the diffusive flux at cloud top becomes negligible while at cloud base it becomes the dominant physical mechanism, balancing both the latent and radiative flux convergences.

The basic feature in the evolution of cirrostratus cloud layers, initially supersaturated within and with subsaturated air below, is that crystals become larger at the cloud top initially before diminishing in size, as a result of decrease in supersaturation and fall into dry air. Crystals are always smaller at cloud base than at cloud top. Growth of ice crystals in supersaturated regimes results in a decrease of the ice saturation ratio, accompanied by a depletion in the ambient vapor field. In our present model where there are no updrafts accompanied by fresh nucleation, the cloud subsides out of the initially supersaturated regime and the cloud top tends to collapse upon the cloud base. The time period of evolution for a single cloud cycle in this study is comparable to the time period obtained in convective cirrus cloud cell models (e.g., Starr and Cox, 1985) for clouds of initially comparable properties. As the cloud evolves, temporal changes occur in the radiation fields, both within and at the cloud boundaries. Due to the dependence of crystal fallspeeds on size, cloud microphysical characteristics become an important determinant of the vertical distance fallen by clouds.

It is somewhat intriguing that a simulation with microphysical details but no convection compares at all with a simulation employing bulk microphysics but detailed convection (Starr and Cox, 1985). Gross cloud behavior may possibly be compared with "bulk" treatments of both cloud dynamics and microphysics. Nevertheless, it is certain that a comprehensive understanding of cirrus clouds will require detailed treatment of both microphysics and convection.

Acknowledgments. The authors thank Drs. J. Coakley, R. Dickinson and J. T. Kiehl for their comments on an earlier draft of the manuscript. We are also indebted to the anonymous reviewers for their suggestions.

APPENDIX A

Radiative Transfer Model

The radiative transfer across the cloud in the solar and the longwave spectra is evaluated using the delta-Eddington approximation. The azimuthally independent equation for any plane-parallel homogeneous layer at any wavelength can be written as

$$\mu \frac{dI}{d\delta} = I(\delta, \mu) - \frac{1}{2}\int_{-1}^{1} d\mu' P(\mu, \mu') I(\delta, \mu') - J \quad \text{(A1)}$$

where μ is the cosine of the zenith angle, δ the optical depth of the layer, P the phase function of the scatters and J the source function. In the solar spectrum,

$$J = \frac{\mu_0 F_0 \omega}{4} \quad \text{(A2)}$$

where μ_0 is cosine of the solar zenith angle and F_0 the incident solar flux, while in the longwave

$$J = (1 - \omega) B(T) \quad \text{(A3)}$$

where B is the Planck function corresponding to the layer temperature.

In the longwave spectrum, we consider the transfer of radiation in the 8–12 μm spectral interval only. We ignore the radiative effects of gases in the cloud layer (Stephens, 1983; Liou, 1974). Radiation is assumed to be incident on the top and bottom of the cloud. With the Eddington approximation

$$I(\delta, \mu) = I_0(\delta) + I_1(\delta)\mu, \quad \text{(A4)}$$

the transfer equation (A1) becomes, for the ith layer

$$I_{0i} = k_{1i} \exp(m_i \delta_i) + k_{2i} \exp(-m_i \delta_i) + B(T_i)$$

$$I_{1i} = \frac{m_i}{(1 - \omega_i g_i)} \quad \text{(A5)}$$

$$\times \left[k_{2i} \exp(-m_i \delta_i) - k_{1i} \exp(m_i \delta_i) - \frac{dB(T_i)/d\delta}{m_i} \right]$$

with $i = 1, 2, \cdots, N$ and

$$m_i^2 = [3(1-\omega_i)(1-\omega_i g_i)], \tag{A6}$$

where k_{1i}, k_{2i} are constants determined from boundary conditions and g_i is the asymmetry factor. To account for phase functions peaked sharply in the forward direction, the single scattering parameters are scaled (Joseph et al., 1976).

The radiation field inside the cloud is completely determined by the sets of $2N$ coefficients (k_{1i}, k_{2i}). The fluxes are given by

$$F_{\downarrow}^{\uparrow}(\tau_i) = \pi[I_{0i}(\delta_i) \pm \tfrac{2}{3} I_{1i}(\delta_i)]. \tag{A7}$$

We need $2N$ equations to evaluate these coefficients. There are two boundary conditions related to the radiative fluxes external to the cloud namely, 1) the radiative flux incident at cloud top [$F^{\downarrow}$ ($\delta = 0$)], and 2) the radiative flux incident at cloud base [$F^{\uparrow}$ ($\delta = \delta_f$)].

The remaining $2N - 2$ conditions are that the intensities be continuous at each of the $N - 1$ levels, i.e.,

$$I_{0i}(\delta = \delta_i) = I_{0,i+1}(\delta = \delta_i) \tag{A8}$$

$$I_{1i}(\delta = \delta_i) = I_{1,i+1}(\delta = \delta_i) \tag{A9}$$

for $i = 1, 2, \cdots, N - 1$.

The fluxes incident at the cloud boundaries are evaluated from the clear atmosphere fluxes incident at the same levels, using the model described in Ramaswamy and Kiehl (1985).

To obtain k_{1i}, k_{2i} from the $2N$ equations, we use the matrix inversion technique approach described by Wiscombe (1977).

The delta-Eddington approach for the solar spectrum is well treated in several earlier investigations (Joseph et al., 1976; Coakley et al., 1983). The methodology for the present problem is similar to the approach in Ramaswamy and Kiehl (1985) with two important differences. Ice cloud single scattering properties replace those of the water cloud. Further, sublayers are introduced in the altitude range where the cloud is present to facilitate a detailed analysis of microphysical processes. The fluxes inside the cloud and at the cloud boundaries are calculated using the matrix inversion approach described in Wiscombe (1977).

APPENDIX B

Cloud Evolution Model

We solve numerically (8) and (9) in each 50 m thick layer, using 1 sec time steps, to investigate the changes in the microphysical and radiative parameters. The radiative boundary conditions are as described in section 3. The radiative energy flux absorbed per particle is determined using (11). The mass of vapor condensed is determined for each layer. New masses are found using (8) and from them new particle lengths. Changes in air and particle temperature and the total depletion of water vapor are calculated independently for each layer. A fall distance is calculated based on the mean fallspeed (Heymsfield, 1972) within that second, resulting in new vertical positions for the layers.

At this point in the calculation, the model cloud has layers of uniform thickness that are irregularly distributed in the vertical. So a linear interpolation scheme is employed and a new array of regularly spaced layers introduced such that layers of uniform thickness are spread between the top of the previous top layer and the bottom of the previous bottom layer. Particle concentrations are adjusted, keeping the total particle number constant if the new layer thickness differs from the old.

The water vapor field is assumed to be fixed in space. Changes to vapor density at a particular altitude are made when particle growth or evaporation occur within a layer at that altitude. The cloud layers fall relative to the vapor field. There is no relative air motion. The cloud layers are assumed to settle in air that is in uniform motion with no accelerations. No nucleation of new particles occurs. Initial experiments with this model have been carried out by Detwiler and Pratt (1984).

REFERENCES

Barkstrom, B. R., 1978: Some effects of 8–12 μm radiant energy transfer on the mass and heat budgets of cloud droplets. *J. Atmos. Sci.*, **35**, 665–673.

Braham, R. R., Jr., and P. Spyers-Duran, 1967: Survival of cirrus crystals in clear air. *J. Appl. Meteor.*, **6**, 1053–1061.

Coakley, J. A., R. D. Cess and F. B. Yurevich, 1983: The effect of tropospheric aerosols on the Earth's radiation budget: A parameterization for climate models. *J. Atmos. Sci.*, **40**, 116–138.

Danielsen, E. F., 1982: A dehydration mechanism for the stratosphere. *Geophys. Res. Lett.*, **9**, 605–608.

Detwiler, A., and R. W. Pratt, 1984: Clear-air seeding: Opportunities and strategies. *J. Wea. Mod.*, **16**, 46–60.

Goody, R. M., 1964: *Atmospheric Radiation. I. Theoretical Basis*, Clarendon Press, 436 pp.

Hall, W. D., and H. R. Pruppacher, 1976: The survival of ice particles falling from cirrus clouds in subsaturated air. *J. Atmos. Sci.*, **33**, 1995–2006.

Heymsfield, A., 1972: Ice crystal terminal velocities. *J. Atmos. Sci.*, **29**, 1348–1357.

——, 1973: Cirrus uncinus generating cells and the evolution of cirriform clouds. Ph.D. thesis, University of Chicago, 286 pp.

——, 1975a: Cirrus uncinus generating cells and the evolution of cirriform clouds. Part I: Aircraft observations of the growth of the ice phase. *J. Atmos. Sci.*, **32**, 799–808.

——, 1975b: Cirrus uncinus generating cells and the evolution of cirriform clouds. Part III: Numerical computations of the growth of ice phase. *J. Atmos. Sci.*, **32**, 820–830.

——, and C. M. R. Platt, 1984: A preliminary parameterization of the particle size spectrum of ice clouds in terms of the cloud temperature and ice water content. *J. Atmos. Sci.*, **41**, 846–855.

Howell, W. E., 1949: The growth of cloud drops in uniformly cooled air. *J. Meteor.*, **6**, 134–149.

Hunt, G. E., 1973: Radiative properties of terrestrial clouds at visible and infrared thermal window wavelengths. *Quart. J. Roy. Meteor. Soc.*, **99**, 346–369.

Joseph, J. H., W. J. Wiscombe and J. A. Weinman, 1976: The delta-Eddington approximation for radiative transfer. *J. Atmos. Sci.*, **33**, 2452–2459.

Liou, K. N., 1973: Transfer of solar irradiance through cirrus cloud layers. *J. Geophys. Res.*, **78**, 1409–1418.

——, 1974: On the radiative properties of cirrus in the window region and their influence on remote sensing of the atmosphere. *J. Atmos. Sci.*, **31**, 522–532.

——, and T. Sasamori, 1975: On the transfer of solar radiation in aerosol atmospheres. *J. Atmos. Sci.*, **32**, 2166–2177.

McClatchey, R. A., R. W. Fenn, J. E. A. Selby, F. E. Volz and J. S. Garing, 1972: *Optical Properties of the Atmosphere*, third ed., AFCRL-72-0497, Air Force Cambridge Research Laboratories, Hanscom AFB, MA, 110 pp.

Manabe, S., and R. T. Wetherald, 1967: Thermal equilibrium of the atmosphere with a given distribution of relative humidity. *J. Atmos. Sci.*, **24**, 241–259.

Paltridge, G. W., and C. M. R. Platt, 1976: *Radiative Processes in Meteorology and Climatology*, Elsevier, 318 pp.

Pruppacher, H. R., and J. D. Klett, 1978: *Microphysics of Clouds and Precipitation*, Reidel, 714 pp.

Ramanathan, V., E. J. Pitcher, R. C. Malone and M. L. Blackmon, 1983: The response of a spectral General Circulation Model to refinements in radiative processes. *J. Atmos. Sci.*, **40**, 605–630.

Ramaswamy, V., and J. T. Kiehl, 1985: Sensitivities of the radiative forcing due to large loadings of smoke and dust aerosols. *J. Geophys. Res.*, **90**, 5597–5613.

Starr, D., and S. K. Cox, 1985: Cirrus clouds. Part I: A cirrus cloud model. *J. Atmos. Sci.*, **42**, 2663–2681.

Stephens, G. L., 1980: Radiative properties of cirrus clouds in the infrared region. *J. Atmos. Sci.*, **37**, 435–446.

——, 1983: The influence of radiative transfer on the mass and heat budgets of ice crystals falling in the atmosphere. *J. Atmos. Sci.*, **40**, 1729–1739.

Warren, S. G., 1984: Optical constants of ice from the ultraviolet to the microwave. *Appl. Opt.*, **23**, 1206–1225.

Welch, R. M., S. K. Cox and W. G. Zdunkowski, 1980a: Calculations of the variability of ice cloud radiative properties at selected solar wavelengths. *Appl. Opt.*, **19**, 3057–3067.

——, —— and J. M. Davis, 1980b: *Solar Radiation and Clouds. Meteor. Monogr.* No. 39, Amer. Meteor. Soc., 93 pp.

Wendling, P., 1980: On the interaction of radiation and cirrus clouds in the infrared window region. *J. Rech. Atmos.*, **14**, 399–407.

Wiscombe, W. J., 1977: The delta-Eddington approximation for a vertically inhomogeneous atmosphere. NCAR Tech. Note. NCAR/TN-121+STR, NCAR, Boulder, 66 pp.